MODELLING SANDWICH FAILURE UNDER BLAST LOADS

Cornelis van 't Hof[1], André G. van Erkel[1], Alexander W.J. Gielen[2]

[1]TNO Defence, Security and Safety, P.O. Box 45, 2280 AA Rijswijk, the Netherlands
[2]TNO Science and Industry, P.O. box 6235, 5600 HE Eindhoven, the Netherlands
cornelis.vanthof@tno.nl

ABSTRACT

Sandwich structures are increasingly applied on naval vessels and mega yachts. At TNO, research into enhancing the blast, shock, ballistic and fire performance of sandwich panels is ongoing. The work presently reported focuses on the validation of a number of failure models for blast loaded sandwich panels fitted into steel joints. Typical failure modes for these constructions are: failure of the adhesive bond between steel and sandwich, core failure, delamination and in-plane (compression) failure of the FRP facings. Failure models for delamination, adhesive bond failure and foam core or filler material failure were developed at TNO over the past decade and were extensively validated for underwater shock. Missing in the toolbox was a model for the in-plane failure of the FRP facings. Recently a continuum damage model for the in-plane failure of non-crimp fabrics was developed. The delamination model and the failure models for foam, adhesive bonds and non-crimp fabrics are validated for use in blast loaded composite structures. The results of simulations were compared to the experimental results of both blast tests on sandwich panels and laboratory tests on GFRP specimens. The general agreement in numerical and experimental observations during the 1st series of blast tests gives confidence in the use of the foam model for blast applications. No firm conclusion for the adhesive bond model could be drawn yet. The predictive capabilities of the in-plane failure model were found excellent for tension but too conservative in case of compression, based on simulations of laboratory tests. A different use of the model is proposed that significantly improved the simulation of the laboratory compression test. This approach was also used to simulate the 2nd series of blast tests, together with the delamination model, a combination which was quite successful in predicting the onset of compressive failure of the blast loaded facing.

1. INTRODUCTION

Composite sandwich structures are increasingly applied on naval vessels and mega yachts. Considerations for the application of sandwich structures are weight reduction, fire insulation, maintenance, radar cross section reduction and functional combinations, such as radar transparency, aperture incorporation, conformal arrays and ballistic incorporation.

At TNO, research into the blast, shock, ballistic and fire performance of sandwich panels with the intent to increase the resilience is ongoing. The work presently reported focuses on the validation of a number of failure models for blast loaded sandwich panels fitted into steel joints. Typical failure modes for these constructions are: failure of the adhesive bond between steel and sandwich, core failure, delamination and in-plane (compression) failure of the FRP facings.

The objective of the research presented is to validate the available failure models for application in blast loaded sandwich structures.

The failure models for delamination, adhesive bond failure and foam core or filler material failure were developed at TNO over the past decade and form together the so-called failure prediction tool or FPT. The FPT was implemented in the explicit finite element code LS-Dyna. These models were extensively validated for underwater shock [1,2].

The FPT's adhesive bond model is characterised by a strain energy failure criterion, the crack direction is perpendicular to the 1st principal stress. The model, using a damage mechanics approach, is implemented in LS-Dyna as a user material.

The failure model for foams is rather similar to the adhesive model, but extended with a compressive crushing plateau. Crushing leaves residual tensile properties unaffected, but tensile damage does affect the crushing properties [3].

The FPT's delamination model has two appearances. The first is an extension of LS-Dyna's contact algorithm; the second is an implementation for orthotropic solids. The criterion for failure initiation is a modified Hashin criterion, a damage mechanics approach is chosen to model failure propagation.

Missing in the above toolbox was a model for the *in-plane* failure of the FRP facings. Recently a continuum damage model for the in-plane failure of non-crimp fabrics (NCF) was developed and implemented in LS-Dyna [4,5]. This model describes laminate failure or degradation by means of matrix failure, fibre tensile failure or fibre kink band failure, under arbitrary 3D stress states.

2. EXPERIMENTAL

2.1 General

All blast tests conducted are performed on TNO's so-called blast simulator [6]. This is a long steel tube which increases step by step in diameter. On the small diameter end, an air-acetylene mixture is detonated in the high-pressure section. Subsequently a blast wave travels through the tube, to arrive more or less planar at the other end, with a diameter of 2 m, were the target surface is mounted. Some characteristic numbers of the maximum blast load are: reflected peak pressure 130 kPa, (positive) phase duration 70 ms. The reproducibility of this test setup is very good.

The aim of the presented test series is to validate a number of material (failure) models. This requires a data regarding the global response and relevant failure modes, e.g. time or deflection at failure, to be compared with the FEA results. In practice, the high speed camera recordings provide the most useful information.

The material (failure) models used in the FE analyses require input in the form of material parameters like moduli, strengths and critical energy release rates G_{Ic}. All relevant material parameters for the foam core, the GFRP facings and the steel – adhesive – GFRP interface were determined by the appropriate standard laboratory experiments. Note that quasi-static experiments were performed only. For the foam – facing interface, interface failure is assumed to be in the foam core.

2.2 Test series

Two test series were performed. In the 1st series the focus was on the FPT foam failure model, in the 2nd series the focus was more on the in-plane NCF failure model.

In the 1st series two sandwich panels of 1.0×0.8 m^2 were tested. The first was subjected to a blast load of ±140 kPa, the second to a blast load of ±110 kPa. As the intention of the test was to load the panel with a significant amount of membrane strains, the two shorter (0.8 m) edges were welded to the flange of the blast simulator. The sandwich consists of a 50 mm PMI foam core (Rohacell 51IG) with e-glass/epoxy facings (VTM 244FRB, ACG). The stacking sequence in each facing is [0°/90°/45°/-45°/0°/-45°/45°/90°/0°] and is composed of unidirectional (UD) and NCF prepregs, by 'vacuum only' curing (no autoclave). The 0°-direction aligns with the span direction. The

sandwich is adhesively bonded to the steel (FE355) profiles by Araldite AV 138M using a HV 998 (Huntsman) curing agent.

Although it was estimated that a 140kPa blast load should introduce a significant amount of damage, the test resulted in an overall failure of all adhesive bonds and a fragmented PMI core. Even the carefully setup high speed camera provided only limited useful information. The second test with a 110kPa blast load produced useful information. Especially the images from the camera provided clarifying data. One of the adhesive bonds between the steel joint and the blast loaded facing failed prematurely: according to our estimates only a fraction of the theoretical strength was present. Post-test inspection showed that the steel surface was left entirely clean, in contrast to the steel surfaces found in the first test. This indicated that surface preparation apparently had not been perfect here, resulting in substandard bonding strength.

The camera's also nicely recorded the formation of characteristic cracks in the foam, with subsequent foam – facing detachment towards the panel centre. One of these is shown in Fig. 1.

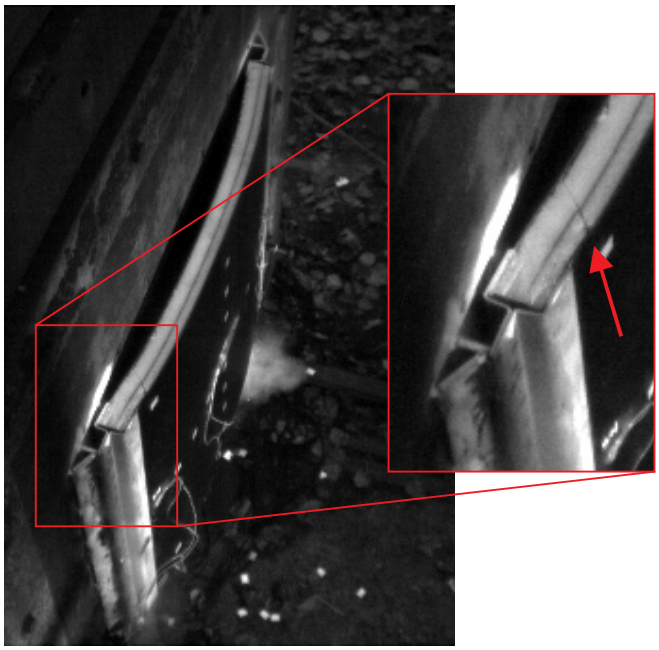

Figure 1: Foam crack arising after 4 ms, as recorded by one of the high speed cameras.

In the 2nd series the objective was to validate the failure model for NCF, developed at Imperial College in London [4,5], for blast purposes. A sandwich was designed by FEA such that compressive failure of the inner facing was likely to occur without face wrinkling, failure in the adhesive bonds or in the foam core. For this purpose the sandwich panels are simply supported, see also Fig. 13. Note that during the design stage only approximate material parameters were available; failure modes like face wrinkling could not be excluded. In contrast to the panels from the 1st series, a different core material, thickness, and facing stacking sequence was chosen. The stacking sequence in the 2nd series panel is [0°/45°/-45°/90°/core/90°/-45°/45°/0°], the core material is PEI (Airex R82.60, Alcan) and its thickness is 30 mm.

In the first test a reflected blast load of 70 kPa was applied. After the test both face wrinkling (i.e. buckling of the facing without failure, but with detachment of the core - facing interface) and crack growth by compressive failure was observed on the blast loaded facing, see also Fig. 2a.

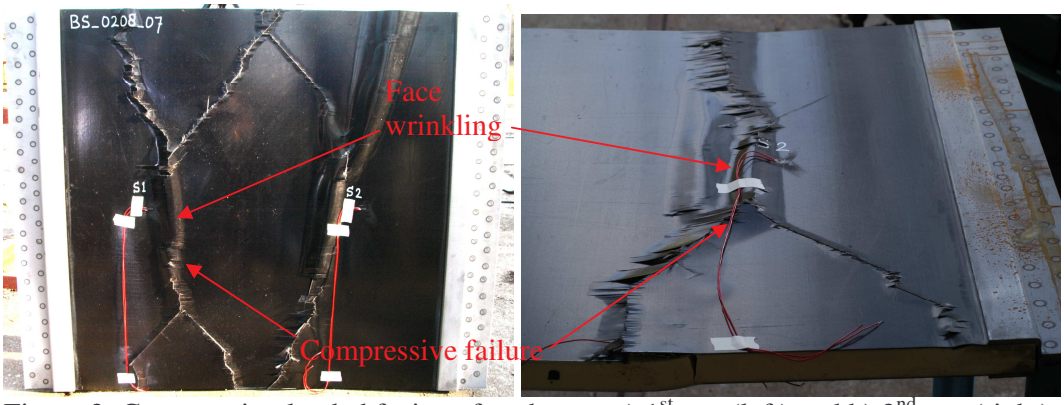

Figure 2: Compression loaded facing after the test a) 1st test (left) and b) 2nd test (right).

In this test failure initiated outside the view of any of the 4 cameras. We anticipated a mid-span failure, as expected for quasi-static loading, but failure initiated closer towards the supports. Note that the compressive cracks progressed along the 45°-direction.

In the 2nd test a reflected blast load of 60 kPa was applied. A similar type of failure was observed, see also Fig. 2b. In this case, the high speed camera recordings were somewhat opaque by mist, probably generated by blast compression of moist air. This mist blurred the failure initiation. Nevertheless, valuable results were obtained during the 2nd test by one of the cameras. The recording rate was 10.000 fps and the most interesting images, from the right hand side of the panel, are shown in Fig. 3. The observations from this image sequence are described in Table 1.

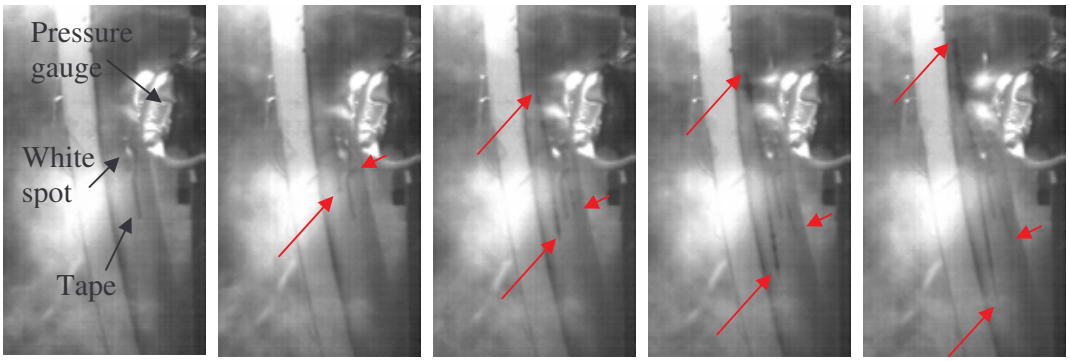

Figure 3: Crack growth in 5 subsequent frames taken at 10.000 fps, i.e. with 0.1 ms in between. Red arrows indicate the crack fronts.

Frame	Time [ms]	Observation
76	4.8±0.1	White spot arises close to strain gauge
77	4.9±0.1	White spot grows
79	5.1±0.1	Damage starts growing from white spot
80	5.2±0.1	Cracks grow towards right hand side (RHS) edge, both up- and downwards. Also a crack grows towards the LHS edge (downwards)
83	5.5±0.1	Upwards growing crack seems to reach RHS edge
84	5.6±0.1	Dust cloud at end of upwards growing crack

Table 1: Observations from high speed video recordings. NB t_0 ~ frame 28.

The 'white spot' observed in the camera recordings probably is a reflection by the face wrinkling more clearly observed after the test. I.e. it is plausible that panel failure was initiated by – undesired – face wrinkling rather than compressive failure of the facing. Nevertheless, cracks due to compressive failure do start to grow from the location where the wrinkle ends, i.e. is still attached to the core, with a preference to the 45°-direction. Note that crack growth rates are of the order of 400 mm / 0.4 ms ≈ 1000 ms^{-1}.

As the results of the 1st test were not fully conclusive, the results of the 2nd test are used to analyse test 1, as this is the test simulated in section 3.3. In test 1 the first sign of failure enters the visible area after 4.9 ms, reaching the panel's edge at 5.0 ms. See also the probable crack growth directions in Fig. 4. Test 2 learned that cracks grow at approximately 1000 ms^{-1}. The distance of about 200 mm to the observed wrinkle took about 0.2 ms; i.e. cracking probably initiated at 4.7 ms. Test 2 also showed that it takes some 0.3 ms from face wrinkling to crack growth, i.e. in test 1 wrinkling probably initiated after 4.4 ms.

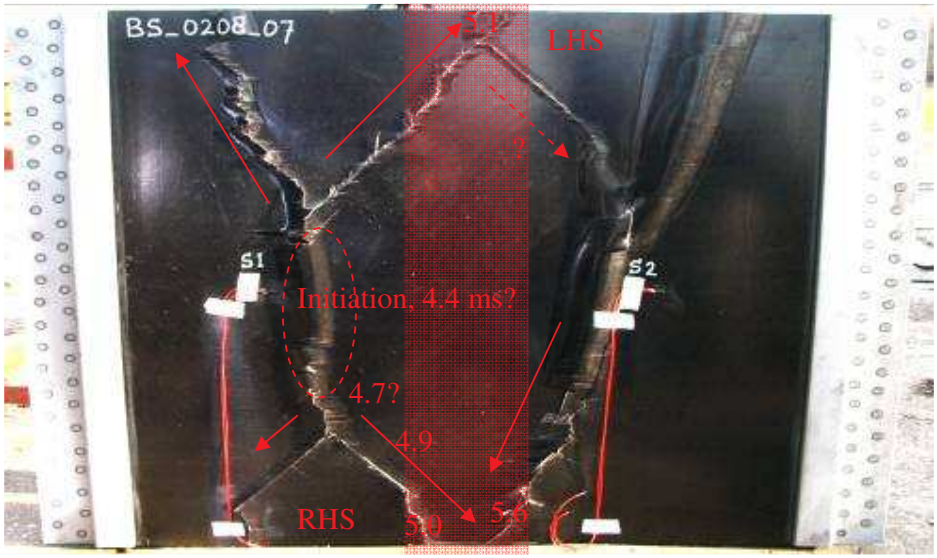

Figure 4: Picture of probable crack growth directions. In transparent red, the approximate view camera on the right hand side.

3. NUMERICAL

The material models used are based on fracture mechanics principles. Mesh dependency of the results is greatly reduced if the element dimensions satisfy a condition dependent on material constants. The energy balance for creating a crack surface A in an element with volume V is

$$\tfrac{1}{2}\sigma_{\max}\varepsilon_{ult}V = G_{ic}A \qquad (1)$$

where $\sigma_{\max}$ the maximum driving stress, ε_{ult} the ultimate driving strain and G_{ic} the appropriate critical energy release rate. For mesh independency $\varepsilon_{\text{ult}} > 2\varepsilon_{\text{ini}}$, where ε_{ini} is the onset failure strain from $\sigma_{\max} = E\varepsilon_{\text{ini}}$, where E is a modulus. Substitution of the last inequality in Eq. 1 gives a restriction for the element dimensions. For example for the GFRP, the in-plane element dimensions should be of the order of 0.5 mm, in case the out-of-plane dimension equals the ply thickness.

3.1 First test series

A 3D FE model was created, shown in Fig. 5. Plane strain conditions were imposed by using only one element in width direction and constraining the out-of-plane displacement. The spot-welds connecting the two halves of the steel joint are modelled by a number of shared nodes between the two steel layers.

Figure 5: Geometry of the FE model representing the sandwich in the 1st test series.

The outer left steel nodes are taken as clamped; on the right hand side symmetry conditions are prescribed. The experimental reflected blast pressure is applied on the top facing. A contact formulation is specified between foam core and the GFRP facings and steel, to prevent unrealistic penetration after core failure. The GFRP facings are modelled using quasi-isotropic representative properties as calculated by the classical laminate theory. This is a good approximation for the global sandwich behaviour. However, the local bending stiffness of the facings is underestimated. This approximation may lead to unrealistic failure behaviour close to joints and therefore needs future attention. Currently this is acceptable as the test and simulations focus on the validation of the foam core failure model. Still, the premature failure of one of the steel-facing interfaces forced us to include the adhesive bond failure model and manually adapt the strength of the failing bond in the FE model. This prevented a firm conclusion with respect to this adhesive bond model.

The foam crack observed by the camera, see Fig. 6, seemed to have been triggered by a local defect in the foam. Upon deletion of one foam element at the defect location the crack was reproduced numerically quite well. One has to take in mind that plane strain simulation actually cannot be used for a defect on the panel's top edge. Therefore, a 3D simulation with a 10 mm deep mesh, sufficiently deep to take into account the 3D redistribution of stress and spatial energy dissipation, was performed. Similar results were obtained with this model, which indicates that the surface crack is representative for the overall panel crack. The overall agreement between simulations and experiments in terms of location, direction, and timing of the crack gives confidence in the foam failure model for blast loaded sandwich structures.

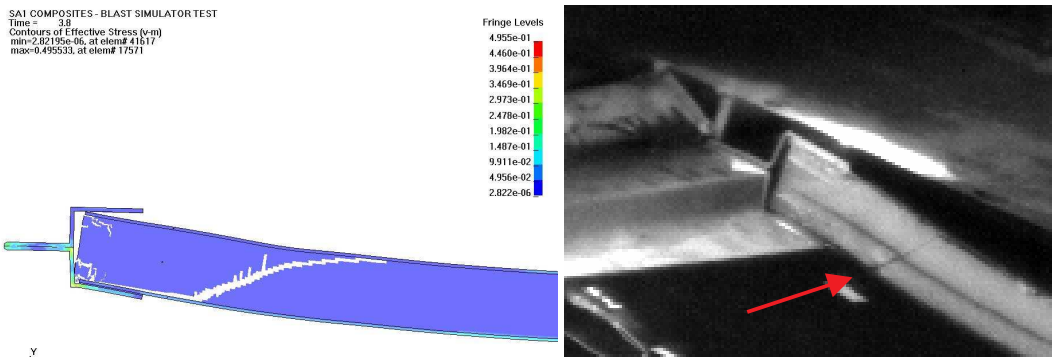

Figure 6: Numerically predicted and experimentally observed crack in the foam core.

3.2 Second test series - preparations

Prior to modelling the full scale blast tests the tension and compression tests for a multi-directional GFRP specimen were simulated using the in-plane NCF failure model.

Fig. 7 shows history variable (HV) 1 in the FE model of the tensile test specimen. HV1 represents the proximity to matrix failure initiation and runs from 0 to 1; in the top ply (45°) of the specimen matrix failure is widely spread. The stacking sequence of the specimen is $[45°,0°,-45°,90°]_{2s}$, where 0° is oriented in loading direction. Every UD ply, approx. 0.25 mm thick, is modelled using a single layer of elements. The tabs, represented in blue, are also GFRP. Loading is applied by prescribed displacement of the tab area 'in contact with the grips'. UD material data is used as input. All material data, both UD, MD and the interlaminar properties, were measured by Risø in Denmark.

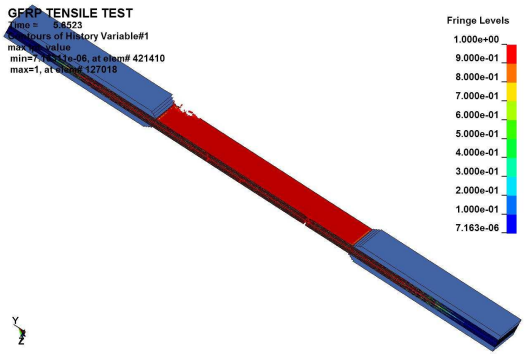

Figure 7: Tensile test specimen from simulation prior to failure.

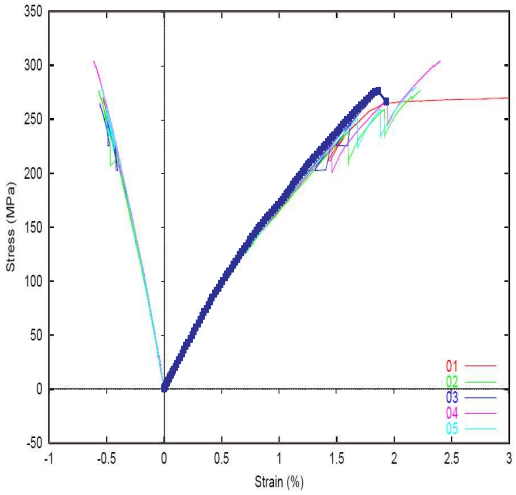

Figure 8: Experimental (1-5) and numerical stress – strain curves.

Experimental stress – strain curves are presented in Fig. 8, for five specimens. Curves on the negative strain axis represent transverse strains. The thick blue line represents the numerical results. Excellent agreement is observed.

Similar simulations were performed for compression tests; see also Figures 9 and 10.

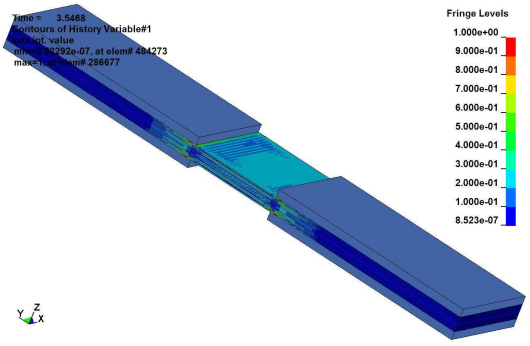

Figure 9: Compression test specimen from simulation prior to failure.

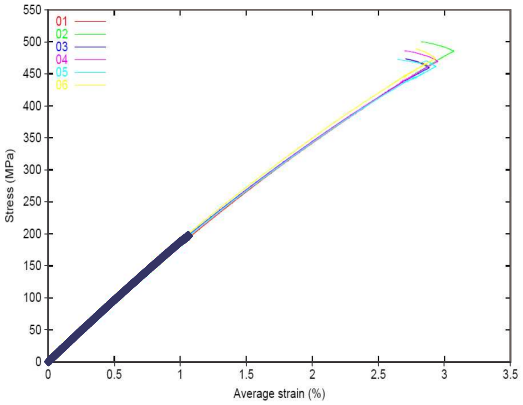

Figure 10: Experimental (1-5) and numerical stress – strain curves.

The stress – strain curves for the compression tests are shown in Fig. 10. Note that the compression strength of the GFRP is higher than the tensile strength!

The numerical stress – strain curve is represented by the thick blue line. As can be seen, the specimen in the simulation fails too early compared to the experiment. Similar results were obtained for a carbon fibre (CF) in a PA6 (Nylon) matrix material system, see the line with red markers in Fig. 11. The early failure is caused by the premature onset of fibre kinking in the failure model. In the model the onset of kink band failure is detected by checking for matrix failure in an area with virtual fibre misalignment, the potential kink band. The premature onset may be due to the fact that only a part of the equilibrium and compatibility equations is used to estimate the state of stress in the kink band [4], actually an orthotropic inclusion in an orthotropic matrix.

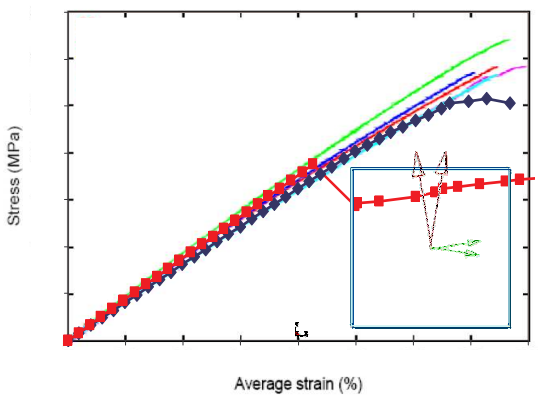

Figure 11: Experimental curves and numerical stress - strain curves (with markers) for CF/PA6.

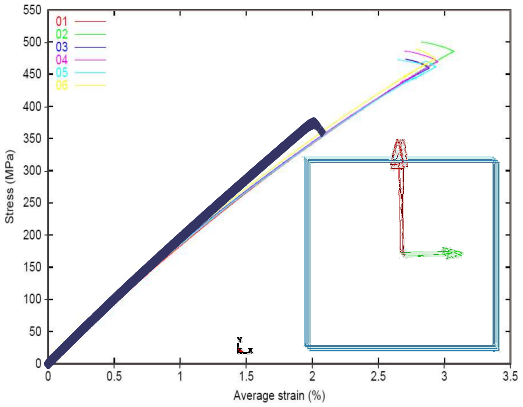

Figure 12: Experimental (1-5) and numerical stress – strain curves, the latter using the 'scattered orthotropy approach'.

In the case of CF/PA6 this mathematical challenge was circumvented successfully by 'physically' introducing kink bands into the FE model; the finite element discretisation was used to randomly introduce misaligned elements into the FE model: scatter was introduced in the orthotropy directions of every element. The scatter is normally distributed around the global orthotropy directions. The standard deviation was derived by inverse modelling using the UD compression strength as input, and can be interpreted as a material parameter. In this approach the original fibre kinking (sub-) model is turned off; only matrix failure or fibre tensile failure are allowed as failure mode; in elements with relatively large misalignment matrix failure may cause fibre kinking to appear. This approach was very successful in the case of CF/PA6, see the line with the blue markers in Fig. 11. The scatter in orientation in two arbitrary 0°-oriented (vertical in figure) elements is also indicated. A similar approach is adopted for the GFRP here. The results by this approach are represented in Fig. 12; the modulus is somewhat overestimated, the predicted strength increases significantly but is still an underestimation of the experimental strength. In this case, the standard deviation of the scatter is 0.8°; the larger deviations are thus approximately 2.5° in that case. This standard deviation is relatively small. For comparison, the value found for CF/PA6 was 7°. This difference probably has to do with the exceptional ratio of compressive strength over tensile strength found for the GFRP.

The effect of an 'in-situ correction' of the transverse strength, as in [7], was also studied but appeared to have only a minor effect.

3.3 Second test series

The face wrinkling observed in the experiment makes the validation of the in-plane failure model somewhat indirect. Nevertheless, the compressive failure initiating from the end of the wrinkling area offers possibilities to validate the model's crack growth predictive capabilities.

In order to model the failure process observed in the blast experiments, a 3D model is required. Because of symmetry a quarter of the panel was modelled. Actually the ±45° NCF lamellae do not share the panel's symmetry planes; assuming symmetry thus is not exactly correct. As a countermeasure to the slightly disturbed deformation state a certain number of GFRP elements from the symmetry lines was not allowed to fail. Based on earlier experiences, this is sufficient to prevent artificial edge effects.

In this simulation the element dimension restriction inevitably has been violated; the required in-plane element lengths of less than 0.5 mm would lead to an unfeasible model size (> 3.000.000 elements). Instead, 1 mm element length (in-plane) was chosen for the compression loaded facing. The resulting quarter panel model still contains over a million elements. The larger elements may lead to relatively brittle element failure, leading in turn to numerical instabilities.

To limit the total number of elements, different element sizes are used for the different constituents. Non-matching meshes are connected via tied contact. Since face wrinkling was observed in the experiment, the foam core and the compression loaded face are attached via a cohesive zone extension of the contact interface, as developed by TNO.

The blast loaded facing, the red top face in Fig. 13, is modelled in detail; every ply is represented by one layer of elements. Each ply is modelled by the NCF failure model, which is essentially linear elastic orthotropic except for the in plane shear modulus. For in-plane shear, a non-linear shear law is implemented. The new 'scattered orthotropy' approach is adopted. The lower GFRP facing, loaded in tension, is modelled as quasi-isotropic linear elastic material. Representative properties are obtained via classical laminate theory. Foam and adhesive are modelled as linear elastic materials. The steel joint is modelled as piecewise linear plastic.

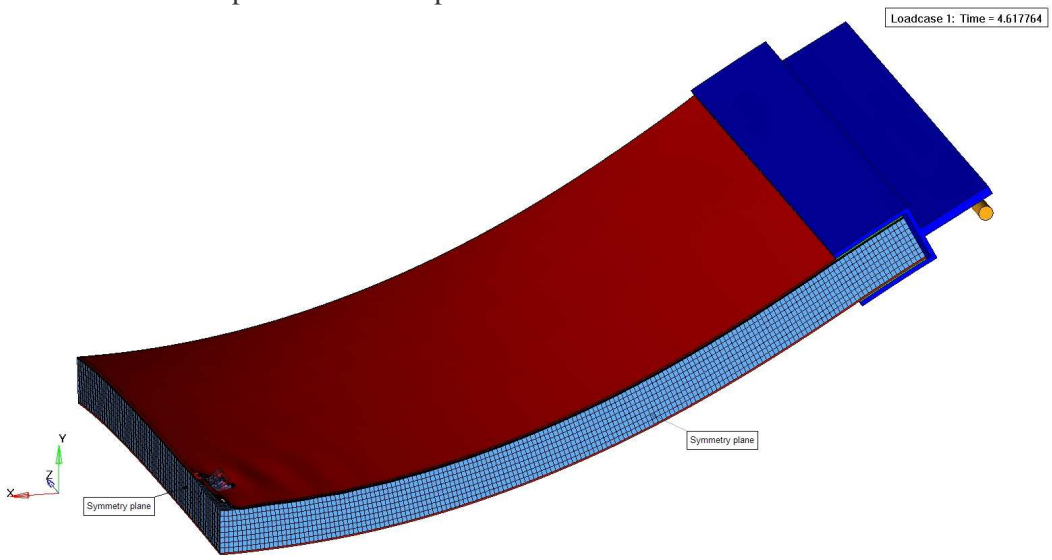

Figure 13: Deflection at end of simulation, scaled by a factor 2.

The experimentally obtained reflected blast load from test 1 is applied in the simulation. The peak reflected pressure is approx. 70 kPa, the (positive) phase duration is some 40

ms. The steel joint is allowed to slide over the steel bar, yellow in Fig. 13, by a contact definition.

To simulate the process with a duration of only 4.6 ms took some 93 hrs CPU time, the time step was approx. 6.7e-5 ms (~ 70 ns). Since the results files for a single time step are approximately 500 MB large, only very limited output was generated.

It is interesting to observe the global deflection. As can be seen in Fig. 13, showing the deflection scaled by a factor two, the panel is doubly curved. The curvature around the x-axis could not be seen on the video recordings. Face wrinkling, as was also observed in the experiment, is clearly visible in Fig. 14, which indicates a well-functioning delamination model. However, unlike in the experiment, this wrinkling starts close to the symmetry plane $x = 0$.

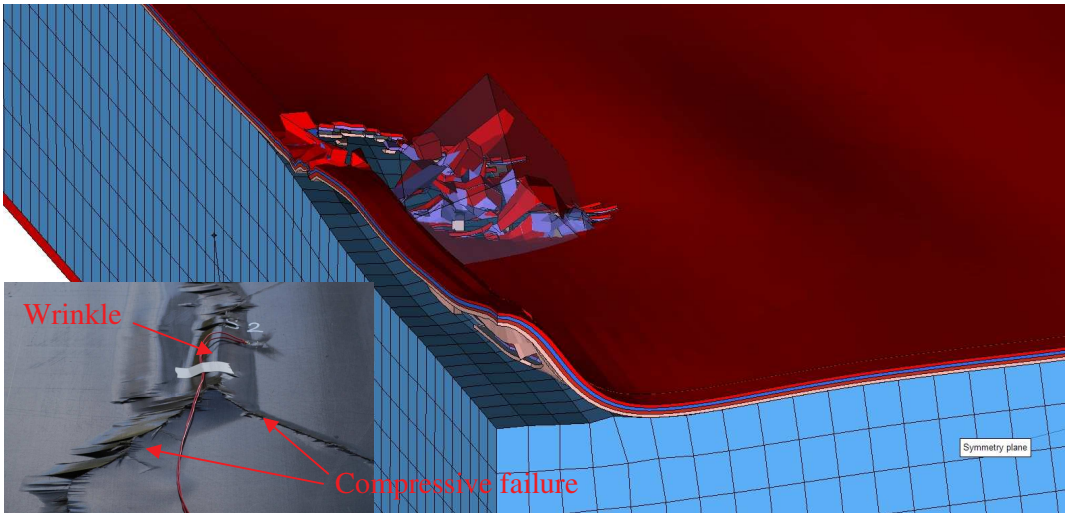

Figure 14: Central face wrinkling and in-plane failure starting at end of wrinkling zone from simulation (detail from Fig. 13) and in the experiment (detail from Fig. 2b).

An important observation is that, like in the experiment, failure of the compression loaded facing starts there were the wrinkle ends; at some z-coordinate the facing is still attached to the foam core and there is where the failure zone is located, see also Figures 15a and 15b, showing the proximity to matrix failure initiation and complete element degradation, respectively.

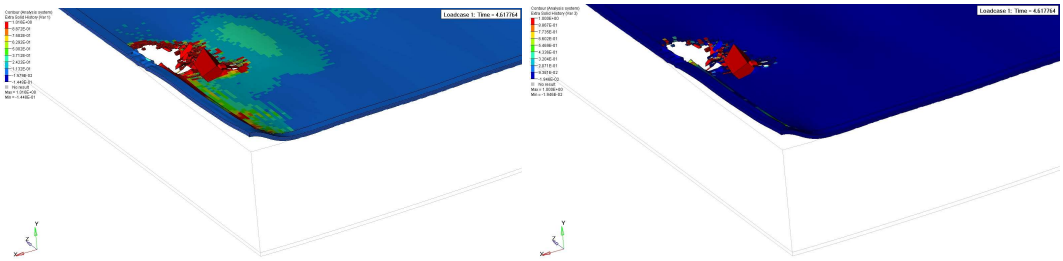

Figure 15: a) HV1 (left) and b) HV4 (right) in the blast loaded facing, the latter representing proximity to ultimate element degradation.

At $t = 4.52$ ms the first core – facing detachment is reported, starting in the panel centre. Given the difference in location of this face wrinkle, timing seems quite in agreement with the experiment. Then at $t = 4.55$ ms the first element fails, and failure continues till 4.62 ms, after which the simulation crashes by numerical instability. The numerical instability, which is also reflected by the relatively large hole created in the failure zone,

is probably due to relatively brittle failure, in turn resulting from violating the element dimension restriction in this simulation. Generally, the combination of the delamination model and the in-plane failure model is quite successful in predicting the onset of compressive failure of the blast loaded facing. In order to study compressive crack growth, the numerical instability needs to be studied in more detail.

4. CONCLUSIONS

TNO developed a toolbox for modelling failure of composite sandwich structures loaded by underwater shock. The toolbox contains models to describe delamination, failure of adhesive bonds and failure of foam cores and is implemented in the FE code LS-Dyna. In the present work these models are validated for use in modelling blast loaded composite structures, by comparing numerical predictions to experimental results of a series of blast tests. General agreement in observed numerical and experimental response/failure gives confidence in the use of these models for blast applications.

A model for in-plane failure was missing in the toolbox. Such a model, for non-crimped fabrics, was developed recently at Imperial College London and was also implemented in LS-Dyna. Based on simulations of laboratory tests the predictive capabilities of this model were found excellent for tension but too conservative in case of compression. A different use of the model is proposed that significantly improved the simulation of the laboratory compression test. This approach was also used to simulate the 2nd series of blast tests, together with TNO's delamination model, a combination which was quite successful in predicting the onset of compressive failure of the blast loaded facing. A study to the capabilities in simulating crack growth is ongoing.

ACKNOWLEDGEMENTS

Dr. Silvestre Pinho (Imperial College London) is kindly acknowledged for allowing TNO to use the LS-Dyna implementation of his model.

REFERENCES

1- Lemmen, P.P.M., Meijer, G.J., and Rasmussen, E.A., *Proceedings of the 70th Shock and Vibration Symposium*, Albuquerque NM USA, 1999.
2- Lesar, D.E. and Gielen, A.W.J., "Validation of a nonlinear plasticity / damage failure model for sandwich structure foam core materials", *Proceedings of the 78th Shock and Vibration Conference*, 2008.
3- Gielen, A.W.J.,"A PVC-foam material model based on a thermodynamically elasto-plastic-damage framework exhibiting failure and crushing", *Int. J. Solids and Structures*, 2008;45:1896-1917.
4- Pinho, S.T., Iannucci, L. and Robinson, P., "Physically based failure models and criteria for laminated fibre-reinforced composites with emphasis on fibre kinking. Part II: FE implementation", *Composites*: *Part A*, 2006;37:766–777.
5- Pinho, S.T., Iannucci, L. and Robinson, P., "Physically-based failure models and criteria for laminated fibre-reinforced composites with emphasis on fibre kinking: Part I: Development", *Composites*, *Part A*, 2006;37:63-73.
6- Haverdings, W., "Evaluation of the 2.0-m diameter blast simulator driven by fuel-oxygen explosive charges", *Proceedings of the 8th Int. Symp. on Military Applications of Blast Simulation*, Spiez, Switzerland, June 1983.
7- Camanho, P.P., Pinho, S.T. et al., "Prediction of in situ strengths and matrix cracking in composites under transverse tensions and in-plane shear", *Composites*: *Part A*, 2006;37:165-176.